Diffraction analysis of highly ordered smectic supramolecules of conjugated rodlike polymers

M. Knaapila, M. Torkkeli, K. Jokela, K. Kisko, L. E. Horsburgh, L-O. Pålsson, O. H. Seeck, I. P. Dolbnya, W. Bras, G. ten Brinke, A. P. Monkman, O. Ikkala and R. Serimaa

conference papers

Diffraction analysis of highly ordered smectic supramolecules of conjugated rodlike polymers

M. Knaapila,[a]* M. Torkkeli,[b] K. Jokela,[b] K. Kisko,[b] L. E. Horsburgh,[c] L-O. Pålsson,[c] O. H. Seeck,[d] I. P. Dolbnya,[e] W. Bras,[e] G. ten Brinke,[fa] A. P. Monkman,[c] O. Ikkala,[a] and R. Serimaa[b]

[a]*Department of Engineering Physics and Mathematics, Helsinki University of Technology, P.O. Box 2200, FIN-02015 HUT, Finland,* [b]*Department of Physical Sciences, P. O. Box 64, FIN-00014, University of Helsinki, Finland,* [c]*Department of Physics, University of Durham, South Road, DH1 3LE, UK,* [d]*Institut für Festkörperforschung, Forschungszentrum Jülich GmbH, D-52452, Jülich, Germany,* [e]*Netherlands Organization for Scientific Research, DUBBLE CRG / ESRF, c/o BP 220 Grenoble F38043, France, and* [f]*Materials Science Center and Laboratory of Polymer Chemistry, University of Groningen, Nijenborgh 4, 9747 AG Groningen, The Netherlands. E-mail: Matti.Knaapila@Helsinki.fi*

A small/wide-angle X-ray scattering and grazing incidence diffraction study of comb-shaped supramolecules of conjugated poly(2,5-pyridinediyl), acid dopant and hydrogen bonded amphiphilic side chains is reported. In solution, polymers are dissolved rodlike particles. When the side-chains are introduced, polymers self-assemble in hierarchic liquid crystals (LC). Diffraction patterns of aligned LC show h00, 020, and 004 reflections, and additional small-angle reflections along the polymer axis. A triangular correlation function indicating a very large correlation length is seen along the smectic axis. An aligned solid structure can be formed by cleaving side chains from the aligned LC.

Keywords: small-angle X-ray scattering; grazing incidence

1. Introduction

The control of structural ordering is essential when designing electro-optical properties of conjugated polymers (Winokur, 1998). Self-assembly, particularly in polyalkylthiophenes, (PAT), results in local order (Tashiro *et al.*, 1991; Prosa *et al.*, 1999; Aasmundtveit *et al.*, 2000) related to improved electronic characteristics, such as high photoluminescence quantum yield (PLQY) (Theander *et al.*, 1999) or charge carrier mobility (Sirringhaus *et al.*, 1999). However, the coiling of PAT resists liquid crystal (LC) and high overall order, and the covalently bonded side chains are permanent. These problems could be overcome with supramolecules of rodlike polymers. Infusible rigid molecules are difficult to align as such and the formation of supramolecules is subtle due to limited mixing entropy. Here supramolecules consist of poly(2,5-pyridinediyl) (PPY), protonated by camphorsulfonic acid (CSA), which leads to efficient PLQY (Monkman *et al.*, 1998) and hydrogen bonded amphiphiles with repulsive alkyl chains, which results in mesomorphism (Knaapila *et al.* 2001a). They assemble in lamellae, in which PPY is organized, with thermotropic and lyotropic character. When required, the side chains can be removed, *i.e.* cleaved, by heating under vacuum (Fig. 1). After alignment in the LC state, the cleaved solid material retains high structural anisotropy with polarized photoluminescence (PL) and high PLQY of pristine polymer (Knaapila *et al.*, 2002a). X-ray diffraction analysis in different stages is presented here.
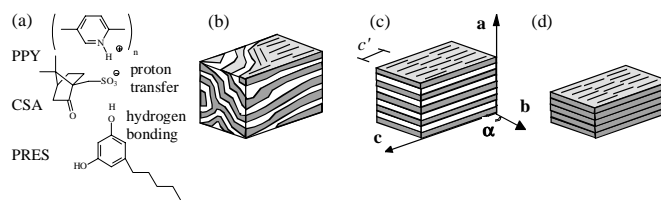

Figure 1
(*a*) Supramolecule of PPY, CSA, and PRES, and their suggested interactions. (*b*) Self-assembled local structure. White layers denote side chains. (*c*) Aligned structure. The structure is characterized by alternating polar and nonpolar layers, the stacking of main chain rings, and the length of the repetition unit of the rigid main chain along **a**, **b**, and **c** axes, in the normal, *equatorial out-of-plane*, almost in the equatorial, *equatorial in-plane*, and in the meridional direction, respectively, forming a monoclinic unit cell with lattice parameters a, b, and c, $\alpha \neq 90°$. Additional order, c', is present along **c** axis corresponding to the tentative length of PPY. (*d*) Solid films where the side chains have been cleaved.

2. Experimental

PPY with random head-to-head and head-to-tail units and Br-ends was prepared by dehalogenation polycondensation of 2,5-dibromopyridine with a triphenylphosphine complex of nickel(0) made *in situ* from reduction of $NiCl_2$ by Zn in the presence of PPh_3 in *N,N*-dimethylformamide. Poly(2,6-pyridinediyl) (PmPY) was made similarly starting from 2,6-dibromopyridine (Horsburgh *et al.*, 1999). Regioregular PPY (rPPY) with 84±6% head-to-tail units was made from 2-bromo-5-iodopyridine, combining organomagnesium and -nickel chemistry (Horsburgh *et al.*, 2002). PPY was complexed by dry CSA to form PPY(CSA)$_x$ in 1 wt.% solutions of formic acid, followed by rapid evaporation and vacuum drying. 5-pentyl-*1,3*-dihydroxybenzene (PRES), 4-hexyl-*1,3*-dihydroxybenzene (HRES), octyl phenol (OP) or 1-octyl-3,4,5-trihydroxybenzoate (OG) were hydrogen bonded to PPY(CSA)$_x$, yielding PPY(CSA)$_x$(amphiphile)$_y$ where x,y are the molar ratios with the respect to the pyridine unit.

The solutions were studied using small-angle X-ray scattering (SAXS) and CuK$_\alpha$ (λ=1.54 Å) radiation from a sealed X-ray tube. The beam was monochromatized with a Ni-filter and a totally reflecting glass block (Huber small-angle chamber 701). The intensity was normalized to the primary beam using a semi-transparent beam stop and measured using a multi-wire proportional counter area detector (HI-STAR). Thick bulk (1 mm), and aligned films (~10 μm) were studied with the same setup. SAXS and wide-angle X-ray scattering (WAXS) patterns were measured using an image plate system from Molecular Dynamics. The beam size was 0.1x0.5 mm², the distance between the sample and the detector was 90 mm and the pixel-size 88x88 μm².

Thick films were also studied at the Dutch-Belgian beam line (BM26B/DUBBLE CRG) at ESRF in Grenoble (France) (Bras, 1998). The beam was monochromatized by the sagittally focusing double crystal Si111 monochromator and the used X-ray energies were 11 and 15 keV. The meridionally focusing coated mirror was used as the second focusing element. Si coating was used for the energies of 11 keV and Pt for 15 keV. The beam size at the sample was 0.35x2.0 mm². The bending radius of the crystal mirror was adjusted to focus the beam at the 2D wire chamber detector. The distance between the sample and the detector was 1.3 or 1.7 m. The WAXS intensity was measured simultaneously using a one-dimensional curved glass microstrip counter with 60° angular range. The q-axis was calibrated using silver behenate and silicon (q is the modulus of the scattering vector, $q = 4\pi\sin\theta/\lambda$ where θ is half the scattering angle).

702 *J. Appl. Cryst.* (2003). **36**, 702–707

Thin films (<100 nm) were studied by GID at the W1.1 (ROEWI) beam line at HASYLAB in Hamburg (Germany). The beam was monochromatized by a double crystal Si(111) monochoromator and the X-ray energy was 10 keV. The beam was focused on the sample and the resulting focus size in the experimental hutch was 1.5x4 mm². The dimension (ver x hor) of the beam was reduced with slits to 0.1x1.5 mm² at the sample. The films were spin-coated onto quartz substrates (1x1 cm²) at 2000 rpm for 30 s from 1 wt.% filtered solutions of formic acid. The samples were mounted on a diffractometer which was designed for surface diffraction with horizontal instrument axis. The sample surface was oriented by means of two translations and two tilts. For GID the diffractometer axis was tilted in the vertical plane. The incident angle was 0.16°. The intensity was measured with a scintillation counter and the incident flux with an ionization chamber. The distance from the sample to the receiving slits was 900 mm.

3. Results and discussion

3.1. Structure in the solution

PPY is soluble in formic acid which does not protonate it unlike CSA. The scattering intensity of PPY in solution is expected to follow that of thin rodlike particles (Kirste & Oberthür, 1982) with cross-terms due to the bromine end-groups,

$$I(q)/I_e V = \frac{c_m N_A}{M_1 L b^2} \Big[(\Delta Z_1)^2 LL_c S_{cc}(qL_c) + 4\Delta Z_1 \Delta Z_{Br} Lb S_{ce}(qL_c) + $$
$$2(\Delta Z_{Br})^2 b^2 J_0(qL) \Big], \tag{1}$$

where $J_0 = \sin(x)/x$ describes the interference between the end-groups. ΔZ_1 and ΔZ_{Br} are the number of excess electrons (per monomer and Br with respect to solvent) and S_{cc} and S_{ce} are the structure factors related to the chain-chain and chain-end interference,

$$S_{cc}(x) = 2(x \operatorname{Si}(x) + \cos(x) - 1)/x^2, \tag{2}$$

$$S_{ce}(x) = \operatorname{Si}(x)/x, \tag{3}$$

where $\operatorname{Si}(x) = \int J_0 dx$. The effect of concentration is included via a cut-off distance L_c beyond which no intra-chain interference is seen,

$$L_c = \frac{2L}{1 + \sqrt{1 + 8\pi \alpha c_m N_A L^2 b / M_1}} \tag{4}$$

where L is the length of polymer, $b=4.35$ Å (Vaschetto et al., 1999) is the repeat unit length and M_1 its molar mass. $N_A = 6 \times 10^{22}$, $\alpha = 0.5$. L_c is based on the criterion that at this radial density c_1 due to other monomers within the same chain around a randomly chosen monomer is proportional to the mass concentration c_m, $c_1(L_c) = \alpha c_m$.

The effect of concentration is rather dominant even for moderate concentrations $c_m \sim 10$ mg/ml. In fact, from equation (4), $c_m^{1/2}L_c \sim 100$ Å (c_m in mg/ml). Therefore, to obtain scattering curves not affected by the concentration e.g. $c_m \sim 4$ mg/ml for $L=50$ Å should be used. The effect is evident at $c_m > 20$ mg/ml in the flat curves which do not exhibit the q^{-1} behaviour expected for rodlike polymers (Fig. 2A). The intensity curves are fairly well expressed with equation (1) indicating that PPY is dissolved without aggregation for $c_m < 8\%$. Based on the whole data set the estimated L of PPY is 50-80 Å. As the persistence length of substituted poly(p-phenylene), an analogous polymer to PPY, is 75-200 Å (Vanhee et al., 1996), this distance is regarded as the length of rodlike sections in PPY as well. L of PPY differs from the $L \sim 300$ Å calculated from the reported $M_w \sim 6000$ g/mol ($M_w/M_n \sim 1.2$-1.6) (Tammer et al., 2002). The reason remains partially open.

Fig. 2(B) gives SAXS intensity curves of PPY, rPPY, PmPY, and PPY(CSA) in formic acid/ethanol solution. Ethanol was added to increase the scattering contrast. It is non-solvent for PPY and causes flocculation at higher mixing ratios. The curves show clear change indicating longer chains and smaller concentration effect. This can be understood by aggregation of the polymers into rodlike bundles whose lengths are at least 300 Å. The aggregates do not grow in a specific direction (such as stacks) indicating that the polymers are not planar at this stage of organization. PmPY on the other hand is coiled in solution. The scattering curve is consistent with a polymer length of ca. 85 Å. That of PPY(CSA)$_{0.5}$ resembles an even more "flexible" polymer with a slope closer to two. Of course, it is not expected that PPY becomes flexible by CSA complexation. Instead, the different slope must be due to aggregation, which due to the bulky CSA group might favor formation of poorly ordered stacks yielding the q^{-2} behavior.
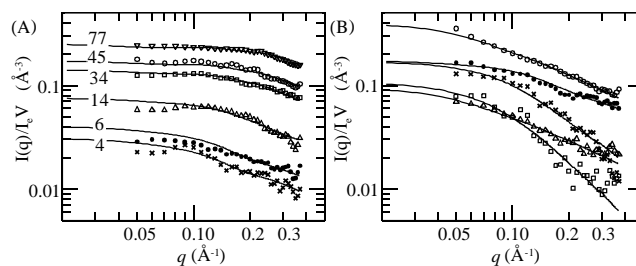

Figure 2
(A) SAXS intensities of PPY in formic acid at concentrations c_m (in mg/ml) as indicated in margin. The solid curves correspond to the model equation (1) with $L = 60$ Å, $\Delta Z_1 = 8.5$ e and $\Delta Z_{Br} = 24$ e. (B) Scattering curves in 80/20 vol/vol formic acid/ethanol for PPY at 30 mg/ml (circles) and 5 mg/ml (triangles), rPPY at 8 mg/ml (dots), PmPY at 8 mg/ml (crosses) and PPY(CSA)$_{0.5}$ (squares). Model [equation (1)] curves for PPY and rPPY: $L=$ 300 Å and 65 Å. Model for PmPY is the chain of 20 monomers with a random 60° kink. Interpolating curve for PPY(CSA)$_{0.5}$ is a Debye coil (Roe, 2000).

3.2. Self-assembled structure and phase behavior

The starting materials are crystalline and amphipiles contain also larger structures. PPY has a monoclinic crystal structure. Chains lie along the unique axis **c** with $\gamma = 108.7°$ (Samuelsen et al., 2001). The units cell contains two coplanar monomer units stacked along the **a** axis either normal to the **a** axis, or parallel with the **b** axis. The x-ray diffraction pattern of PPY shows 100, 020, and slightly asymmetric 002 reflections at 1.14 Å⁻¹, 1.78 Å⁻¹, and 3.11 Å⁻¹, respectively.

PPY(CSA)$_x$, is an infusible solid with a layer structure of moderate quality due to the bulky CSA. The diffraction pattern of PPY(CSA)$_{0.5}$ reveals peaks at 0.35 Å⁻¹, 1.08 Å⁻¹, 1.4 Å⁻¹, 1.78 Å⁻¹ and 3.1 Å⁻¹. The structure seems to be related e.g with layered H$_2$SO$_4$ intercalated poly(p-phenylenevinylene) (Mao et al., 1998). This is supported by the fact that the reflections due to the polymer stacks (1.78, 3.1 Å⁻¹) are preserved with the "intercalant" CSA layer.

The further complexation of amphiphiles results in proper mesomorphism described by axes **a**, **b**, and **c** (Fig. 1). For instance with alkylresorcinols, for small x, y, e.g. $x=0.25$, $y=0.25$-0.5, a glassy birefringent material is obtained at 25-200 °C. X-ray diffraction reveals very sharp h00 reflections from the lamellar structure, an amorphous halo arising from inter- and intrachain short-range order at ca. 1-1.5 Å⁻¹, a sharp 020 reflection arising from the polymer stacks superimposed on the amorphous halo near 1.8 Å⁻¹, and, depending on the composition, a reflection 004, at 3.0-3.2 Å⁻¹, and an additional broad reflection at 0.09 Å⁻¹ due to order along the rodlike chain.

For higher values, $x=y=0.5$, a frozen-in LC phase is observed at 25°C and at moderate heating, a birefringent fluid is formed with a broad endothermic DSC rise, typical for noncrystalline materials. Simultaneously, the degree of order reaches its maximum decreasing with further increase of x,y, as revealed by the broadening of reflections 100 and 020. In particular, higher complexation ($x,y >1$) results in a gradual destruction of the π-stacking, but also the LC even at 25°C and other phase regime: For $x,y\sim1$ an order-disorder transition (ODT) to an isotropic (non-birefringent) disordered fluid occurs between 140-180°C and a gradual drop in scattering intensity (c.f. Fig. 3A) with an abrupt increase of the width of the $h00$ reflections (Fig. 3B) being observed. The decrease in the long period (Fig. 3C) may be related to an incomplete packing. The loss of interpolymer order within the lamellae is seen slightly below the ODT and the intensity of reflection 020 drops (Fig. 3D-E). These phase transitions are reversible. The structure improves by an initial slow heating-cooling cycle, *i.e.* annealing, possibly due to release of strain and increase in the size of crystallites, like in poly(3-octylthiophene) (Aasmundtveit *et al.*, 2002). Note that such structure improvement is not permanent in e.g. poly(3-dodecylthiophene) (P3DT) (Tashiro *et al.*, 1991). Annealing can also shift peaks as seen in other thermotropic rigid polymers (Sauer *et al.*, 1987). If $y/x\geq2$, the macrophase separation is usually observed.
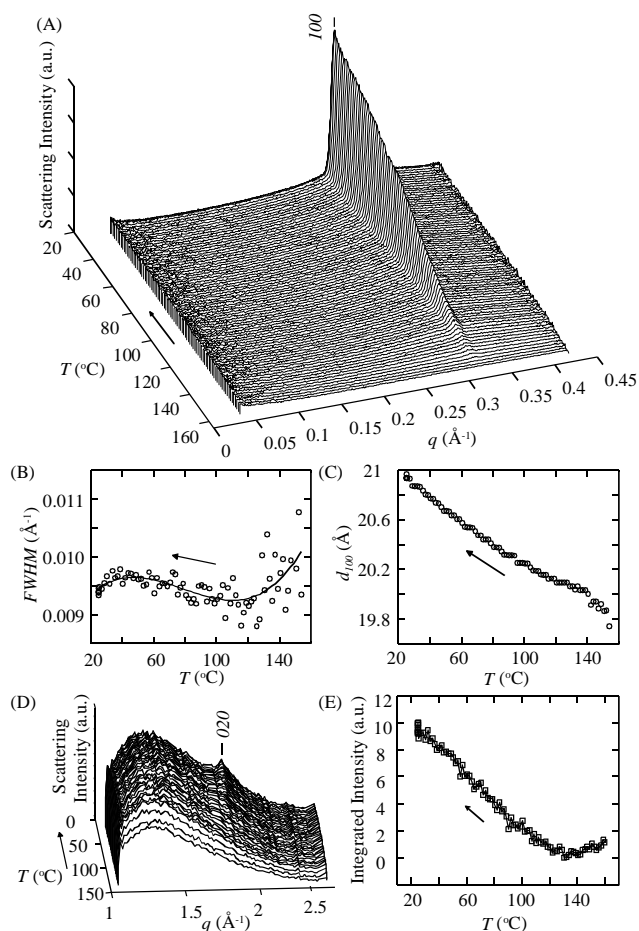

Figure 3
(A) SAXS pattern of PPY(CSA)$_{0.75}$(PRES)$_{1.5}$ during cooling (5 K/min). (B) Full-width half maximum (FWHM) of the reflection 100 showing order-disorder transition from the disordered (isotropic) fluid to the self-assembled (smectic LC) fluid at 140°C. (C) Lamellar period. (D) Simultaneously measured WAXS pattern and (E) integrated intensity of the reflection 020.

All amphiphiles behave similarly but OP tends to phase separate more easily. Regular rPPY and chiral CSA may favour the crystallinity and suppress the mesomorphism though the complexes of rPPY and chiral CSA were found to be quite similar to those of PPY and CSA. Instead, with PmPY, or poly(4-vinylpyridine), due to the coiling, the 100 reflection is much weaker and the reflection 020 arising from the intralamellar structure is absent.

3.3. Aligned self-assembled structure

Cast films were sheared in the *in-plane* direction on the smooth quartz surface. The layers are expected to align along the surface in accordance with cast PPY (Samuelsen *et al.*, 2001) and PPY within the layers with their **c** axis in the drawing direction. X-ray diffraction patterns were measured *ex-situ* in three directions, parallel to the shearing, **x**, perpendicular to the shearing and the surface, **y**, and normal to the surface, **z**. The degree of alignment, indicated by the angular spreads of the reflections easily gives results comparable with the aligned PAT (Tashiro *et al.*, 1991).
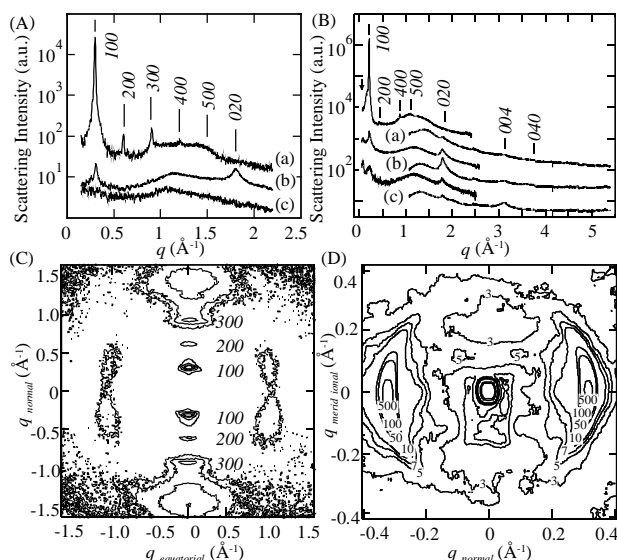

Figure 4
(A) X-ray diffraction curves of aligned PPY(CSA)$_{0.5}$(HRES)$_{0.5}$ and (B) PPY(CSA)$_{0.5}$(OP)$_{1.0}$ (Knaapila *et al.*, 2002*b*) in three directions: (*a*) Normal, **x**. (*b*) Equatorial, **y**. (*c*) Meridional, **z**. The flat halo between 1-1.5 Å^{-1} in (A) is related to an internal structure along the **a** axis corresponding to a period of 4 Å. (C) 2-D X-ray diffraction pattern of PPY(CSA)$_{0.5}$(PRES)$_{0.5}$ after subtraction of amorphous background and polarization and flat field corrections. 2-D X-ray diffraction pattern of aligned PPY(CSA)$_{0.5}$(OP)$_{1.0}$, (D), shows a parallel scattering wall along the **z** axis. The same feature is marked with an arrow in (B).

The $h00$ reflections are parallel to the **x** axis, the 020 almost parallel to the **y** axis, and the 004 and the faint 002 parallel to the **z** axis. PPY stack planes are parallel to the surface and the spacing (3.55 Å) describes the stacking distance, which is nearly the same as in pure PPY (Samuelsen *et al.* 2001). The 004 reflection is related to the intrachain distance of the pyridines and assigned as such since the Bragg distance (~ 2.1 Å) corresponds to one fourth of the length of the suggested PPY(CSA)$_{0.5}$ repeat unit.

The 020 reflection is directed slightly off the (yz) plane and the reflection arc is much wider than those of the $h00$ reflections. In bulk samples, 020 is asymmetric due to the unresolved $h20$ reflections (c.f. Mao *et al.*, 1998). If the alignment is incomplete here, these may project on the (xz) plane and account for the observed widening. Also the absorption of the film suppresses the intensity in the (yz)

plane. The layers are free-floating under pressure implying freedom of the chains stacked in the lamellae. This explains the absence of the non-axial $hk0$ reflections. However, both $h00$ and 020 show well-defined arcs suggesting two-dimensional order in the $(hk0)$ plane. To account for the mesomorphism and the absence of $hk0$ peaks, both the layers and the stacks are assumed to undulate as in the paracrystalline model.

Table 1
Observed Bragg distances corresponding to the suggested lattice parameters, $a=d_{100}$, $b=d_{010}/\sin\alpha$, $c=d_{001}/\sin\alpha$, $\alpha=\arcsin(2d_{004}/4.35\ \text{Å})$, $\beta=\gamma=90^{\circ}$.

Complex	d_{100} (Å)	d_{020} (Å)	$2d_{004}$ (Å)	d'_{001} (Å)	α ($^{\circ}$)
PPY(CSA)$_{0.25}$	19.1	3.54	4.04	63	68
PPY(CSA)$_{0.5}$	18.2	3.5	n.d.	-	n.d.
PPY(CSA)$_{0.75}$	18.7	3.59	4.11	-	71
PPY(CSA)$_{1.0}$	19.0	3.55	4.13	-	72
PPY(CSA)$_{0.25}$ (PRES)$_{0.25}$	18.5	3.49	4.03	63	68
PPY(CSA)$_{0.25}$ (PRES)$_{0.5}$	19.6	3.48	4.04	-	68
PPY(CSA)$_{0.5}$ (PRES)$_{0.5}$	19.5	3.46	4.07	-	69
PPY(CSA)$_{0.5}$ (PRES)$_{1.0}$	20.0	3.45	4.12	-	71
PPY(CSA)$_{0.75}$ (PRES)$_{0.75}$	18.8	3.44	4.09	-	70
PPY(CSA)$_{0.75}$ (PRES)$_{1.5}$	20.6	-	4.14	-	72
PPY(CSA)$_{1.0}$ (PRES)$_{0.25}$	18.6	-	4.11	-	71
PPY(CSA)$_{1.0}$ (PRES)$_{0.5}$	18.2	-	4.16	-	73
PPY(CSA)$_{1.0}$ (PRES)$_{0.75}$	18.6	-	4.16	-	73
PPY(CSA)$_{1.0}$ (PRES)$_{1.0}$	19.2	-	4.16	-	73
PPY(CSA)$_{1.0}$ (PRES)$_{1.5}$	20.1	-	4.16	-	73
PPY(CSA)$_{1.0}$ (PRES)$_{2.0}$	20.4	-	4.17	-	73
PPY(CSA)$_{0.25}$(HRES)$_{0.25}$	20.5	3.48	4.04	64	68
PPY(CSA)$_{0.25}$ (HRES)$_{0.5}$	20.6	3.47	4.03	-	68
PPY(CSA)$_{0.5}$ (HRES)$_{0.5}$	20.1	3.47	4.13	-	72
PPY(CSA)$_{0.5}$ (HRES)$_{1.0}$	n.d.	-	4.14	-	72
PPY(CSA)$_{0.75}$(HRES)$_{0.75}$	18.9	-	4.13	-	72
PPY(CSA)$_{0.75}$ (HRES)$_{1.5}$	20.3	-	4.15	-	73
PPY(CSA)$_{1.0}$ (HRES)$_{0.25}$	19.0	3.53	4.17	-	73
PPY(CSA)$_{1.0}$ (HRES)$_{0.5}$	18.9	-	4.13	-	72
PPY(CSA)$_{1.0}$ (HRES)$_{0.75}$	18.9	-	4.18	-	74
PPY(CSA)$_{0.5}$ (OG)$_{0.5}$	23.3	3.41	4.12	-	71
PPY(CSA)$_{0.5}$ (OG)$_{1.0}$	27.4	3.45	4.15	-	73
PPY(CSA)$_{0.5}$ (OP)$_{1.0}$	25.7	3.50	4.05	63	69

The supramolecular hierarchy with a third level of organization is seen in the diffraction patterns as a reflection at 0.09 Å^{-1} along the **c** axis simultaneously with the previously described features. Reflections at 0.09 Å^{-1} are seen for $x,y \leq 0.25$, where their appearance is concomitant to the broadening of $h00$. When $x,y \sim 0.5$ the peak may also appear upon heating. In the fluid-like PPY(CSA)$_{0.5}$(OP)$_{1.0}$ these reflections appear as parallel streaks akin to nematic liquid systems of relatively monodisperse rodlike molecules, *i.e.* the positional order only along the **c** axis leads to the streaks rather than arcs. The nematic order in this sample differs from that of the remaining samples possibly due to the π stacks. Monodisperse rodlike polymers (Yu *et al.*, 1997) or oligomers (Dupont *et al.*, 2000) can form structures where the chains are in planes corresponding to the length of the chains. The spacing is comparable to the tentative length of PPY and also with the correlation length deduced from the 004. In the tentative idea (Fig. 1*c*) PPY is organized in direct end-to-end manner due to the formation of π-bonded stacks which cannot accommodate the Br-end groups. The polydispersity results in less densely filled and less ordered zones which may contain residual dopant and amphiphiles. PPY is not tilted within these layers, because it is polydisperse and because both **c** axis and reflection at 0.09 Å^{-1} are found along the **z** axis.

In addition to the sharper reflections, broader reflections are seen at 1.08 Å^{-1} and 1.4 Å^{-1} (Fig. 5A&E), present also in PPY(CSA)$_x$. The

first forms a ring in the (yz) plane being related to the weak ordering of CSA within the layers, while the second is seen around the **x** axis having the same orientation distribution as the $h00$. The peak at 1.4 Å^{-1} is sharp for small x behaving in the opposite way as $h00$.

In view of similarities with PPY, a monoclinic unit cell for the complex is suggested instead orthorhombic (Knaapila *et al.*, 2002*a*). The main argument is that d_{001} is ca. 4.05 Å instead of the repeat distance of PPY (4.25 Å (Samuelsen *et al.*, 2001) or 4.35 Å (Vaschetto *et al.*, 1999). Therefore, **a** axis is suggested to be unique and $\alpha \sim 70$-85°. The triclinic structure cannot be excluded, however. Increase of x,y leads to loss of registry between the stacks and finally within the stacks and the structure approaches orthorhombic where d_{020} decreases as the PPY plane becomes normal to the **b** axis and d_{002} approaches the length of pyridine. The interlayer distance $a=d_{100}$ depends on the side-chain length and concentration, as expected, but does not follow the simple scheme of side-chain tilt and interdigitation, while d_{020} and d_{004} as well as the period deduced from the reflection at 0.09 Å^{-1}, d'_{001}, are nearly independent, which supports the proposed picture. With OP and OG, d_{100} is much larger than that of PPY(CSA)$_{0.5}$ unlike alkylresorcinols (Table 1).
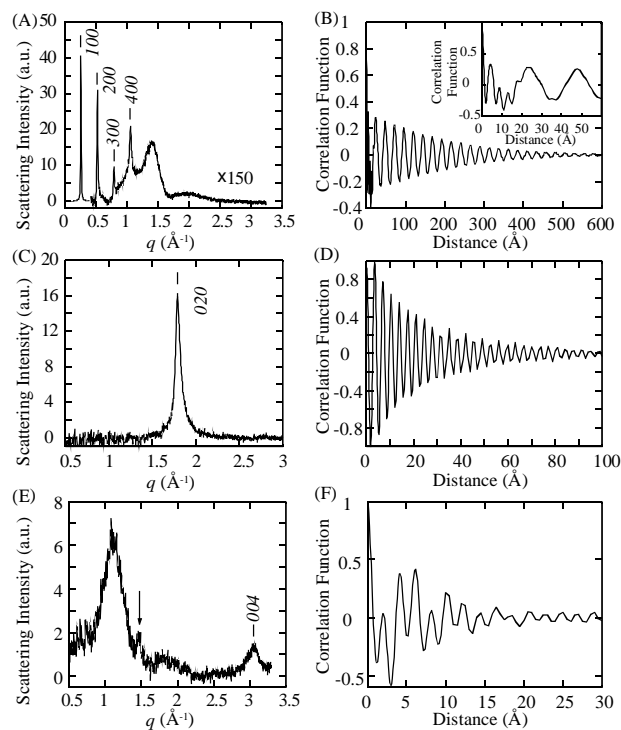

Figure 5
Scattering intensity curves (left) and the correlation functions normalized to $\gamma(0)=1$ (right) of aligned PPY(CSA)$_{0.5}$(OG)$_{0.5}$ (q-range 0-3.3 Å^{-1}) in three directions: (A, B) Normal, **x**. (C, D) Equatorial, **y**. (E, F) Meridional, **z**. The feature marked with an arrow was not identified.

The complexes show excellent local order. The linear correlation function along the coordinate axes, $\gamma_j(r)$, where $j=$**x, y,** or **z**, was calculated from the differential scattering intensity, $I_{j} = I(q_j)-I_{\text{iso}}(q_j)$,

$$\gamma_j(r) = \int q_j^2 I_j(q_j)\cos(q_j r)\mathrm{d}q_j \qquad (5)$$

where $I_{\text{iso}}(q_j)$ is the isotropic intensity due to amorphous material and r is the distance.

Fig. 5 shows I_j and $\gamma_j(r)$ for one example. The background is low and does not affect positions or FWHM of the peaks. Along the **a** axis (Fig. 5A-B) the sharp $h00$ reflections result in a triangular or sinusoidal form of $\gamma_x(r)$ which damps out very slowly with large

correlation length. This indicates highly ordered packing of lamellae and/or a narrow lamellar distribution. The alternating layers produce the main maxima in $\chi_x(r)$ whose separation is d^c_{100}=24 Å being nearly the same as obtained from the bulk sample. The inset (Fig. 5B) shows features of $\chi_x(r)$ at small r, not seen in other directions, arising from the features at 1.4 Å^{-1}, possibly related to short-range order of the sublayers formed by the compounds of the supramolecules. Along the **b** axis (Fig. 5C-D) the only diffraction peak and the periodicity of $\chi_x(r)$ correspond to the stacking period while along the **c** axis (Fig. 5E-F) $\chi_x(r)$ shows two distinct peaks, ~4 Å and ~6.5 Å corresponding to the order of pyridine rings and intralamellar CSA (1.08 Å^{-1}), respectively.

Table 2

The correlation length $L_{hkl}=\alpha\lambda/(\Delta 2\theta\cos\theta)$ and the degree of order D_{hkl}; 2θ is the scattering angle, λ the wave-length of the X-ray, and Δ the width (in radians) of the peak associated with the (hkl) planes. The shape factor, α, is 1 for the infinite lamellae. The instrumental function due to the beam divergence and the spatial resolution of the detector was taken into account. (n.d.= not determined)

Complex	L_{100} (Å)	L_{020} (Å)	L_{004} (Å)	D_{100}	D_{020}	D_{004}
PPY(CSA)$_{0.25}$	170	n.d.	39	8.9	n.d.	n.d.
PPY(CSA)$_{0.25}$(HRES)$_{0.5}$	180	97	32	9.0	28.0	n.d.
PPY(CSA)$_{0.25}$(PRES)$_{0.25}$	200	102	50	10.5	29.2	9.5
PPY(CSA)$_{0.5}$	438	145	37	24.3	41.0	9.3
PPY(CSA)$_{0.5}$ (OG)$_{0.5}$	790	100	32	32.9	37.2	7.9
PPY(CSA)$_{0.5}$ (OP)$_{1.0}$	750	96	30	26.9	27.3	7.4
PPY(CSA)$_{0.5}$ (HRES)$_{0.5}$	670	104	27	31.4	29.9	n.d.
PPY(CSA)$_{0.5}$ (PRES)$_{0.5}$	760	71	28	36.8	29.2	6.9

The correlation lengths, L_{100}, are very large corresponding to tens of well-defined layers (Table 2) as defined by the number of repeat distances, D_{100}, obtained from the peak-width/position ratio. Also excellent stacking order is seen, while the meridional direction is less ordered. Furthermore, the widths of the higher order reflections $h00$ are nearly linearly dependent on q. Therefore, the reflection broadening is principally due to lattice parameter fluctuations (microstrains) and the actual crystallite size may be far higher. This order is better than that of PAT:s, such as poly(3-hexylthiophene) (P3HT) (Aasmundtveit *et al.*, 2000), or P3DT (Prosa *et al.*, 1999), or rodlike poly(oxy-1,4-phenyleneoxy-1,4-phenylenecarbonyl-1,4-phenylene) oligomers (Dupont *et al.*, 2000).

3.4. Self-assembled and cleaved structure in thin films

GID patterns reveal the same structural features in spin-coated films. The layers align parallel to the quartz surface, and the $h00$ maxima are found in the *out-of-plane* direction (Fig. 6a) (Knaapila *et al.*, 2001b). Reflections 020 and 004 are oriented *in-plane* (Fig. 6b). This resembles regioregular P3HT (Sirringhaus *et al.*, 1999) though no self-organization promotor is used here, unlike in the case of P3HT.

The side groups can be cleaved in vacuum (Fig. 1) as revealed by FTIR spectra. The aligned cast films remain optically anisotropic as revealed by polarized PL *i.e.* the alignment of the polymer chains is not lost upon cleavage (Knaapila *et al.*, 2002b). For spin-coated films also CSA can be removed and the cleaved films (Fig. 6c-d) reveal diffraction patterns like PPY (Fig. 6e-f) which align **c** axis along the surface. PPY does not undergo thermal degradation.

4. Concluding remarks

Supramolecules of rodlike PPY were synthesized with highly ordered hierarchic micro- and macrostructures which have not hitherto been reported in conjugated polymers. Materials allow phase tailoring all the way from crystals to disordered liquids, which is uncommon, as a LC is difficult to achieve using general solvents.
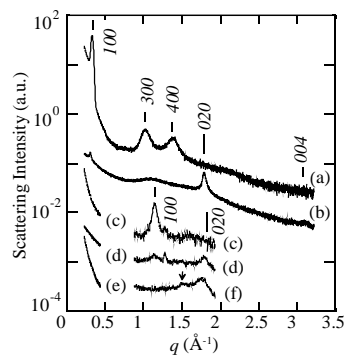

Figure 6

GID patterns of PPY(CSA)$_{0.5}$(PRES)$_{0.5}$, (a-b), d_{100}~19 Å, d_{020}=3.51 Å, L_{020}=130 Å, d_{004}=4.07 Å, L_{004}=70 Å, PPY(CSA)$_{0.5}$(PRES)$_{0.5}$ after heating at 120 °C *in vac* (~ 10^{-3} mbar) for 72 h, (c-d), and pure PPY, (e-f). *Out-of-plane*: (a), (c), and (e). *In-plane*: (b), (d), and (f).

The side groups can also be regarded as specific solvents with high solubility, due to matching bonds. The LC can be induced by varying both the temperature and the concentration of PPY and therefore the system has both thermotropic and lyotropic character.

References

Aasmundtveit, K. E., Samuelsen, E. J., Guldstein, M., Steinsland, C., Flornes, O., Fagermo, C., Seeberg, T. M., Pettersson, L. A. A., Inganäs, O., Feidenhans'l, R. & Ferrer, S. (2000), *Macromolecules, 33*, 3120-3127.

Bras, W. (1998), *J. Macromol. Sci. Phys.,* **B37**, 557-566.

Dupont, O., Jonas, A. M., Nysten, B., Legras, R., Adriaensens, P. & Gelan, J. (2000), *Macromolecules, 33*, 562-568.

Horsburgh, L. E., Monkman, A. P. & Samuel, I. D. W. (1999), *Synth. Met.,* **101**, 113-114.

Horsburgh, L. E., Monkman, A. P., Wang, C. & Bryce, M. R. (2002), *Mat. Res. Soc. Symp. Proc.,* **665**, 169-174.

Kirste, R. G. & Oberthür (1982), *Small Angle X-ray Scattering,* edited by Glatter, O. & Kratky O., pp. 387-431. London: Academic Press.

Knaapila, M., Ruokolainen, J., Torkkeli, M., Serimaa, R., Horsburgh, L., Monkman, A. P., Bras, W., ten Brinke, G. & Ikkala, O. (2001a), *Synth. Met.,* **121**, 1257-1258.

Knaapila, M., Torkkeli, M., Mäkelä, T., Horsburgh, L., Lindfors, K., Serimaa, R., Kaivola, M., Monkman, A. P., ten Brinke, G. & Ikkala, O. (2001b), *Mat. Res. Soc. Symp. Proc.,* **660**, JJ5.21.1-6.

Knaapila, M., Ikkala, O., Torkkeli, M., Jokela, K., Serimaa, R., Dolbnya, I. P., Bras, W., ten Brinke, G., Horsburgh, L. E., Pålsson, L-O. & Monkman, A. P. (2002a), *Appl. Phys. Lett.,* **81**, 1489-1491.

Knaapila, M., Torkkeli, M., Pålsson, L-O., Horsburgh, L. E., Jokela, K., Dolbnya, I. P., Bras, W., Serimaa, R., ten Brinke, G., Monkman, A. P. & Ikkala, O. (2002b), *Mat. Res. Soc. Symp. Proc.,* **725**, 237-242.

Mao G., Winokur, M. J. & Karasz, F. E. (1998), *Phys. Rev. B,* **58**, 4089-4094.

Monkman, A. P., Halim, M., Samuel, I. D. W. & Horsburgh, L. E. (1998), *J. Chem. Phys.,* **109**, 10372-10378.

Prosa, T. J., Moulton, J., Heeger, A. J. & Winokur, M. J. (1999), *Macromolecules, 32*, 4000-4009.

Roe, R-J., (2000) *Methods of X-Ray and Neutron Scattering in Polymer Science.*, Oxford: Oxford University Press.

Samuelsen, E. J., Monkman, A. P., Pettersson, L. A. A., Horsburgh, L. E., Aasmundtveit, K. E. & Ferrer, S. (2001), *Synth. Met.,* **124**, 393-398.

Sauer, T. H., Wendorff, J. H. & Zimmermann, H. J. (1987), *J. Polym. Sci. B: Polym. Phys.,* **25** 2471-2485.

Sirringhaus, H., Brown, P. J., Friend, R. H., Nielsen, M. M., Bechgaard, K., Langeveld-Voss, B. M. W., Spiering, A. J. H., Janssen, R. A. J., Meijer, E. W., Herwig, P. & de Leeuw, D. M. (1999), *Nature*, **401**, 685-688.

Tammer, M., Horsburgh, L., Monkman, A. P., Brown, W., Burrows, H. D. (2002), *Adv. Funct. Mat.*, **12**, 447-454.

Tashiro, K., Ono, K., Minagawa, Y., Kobayashi, M., Kawai, T. & Yoshino, K. (1991), *J. Polym. Sci. B: Polym. Phys.,* **29**, 1223-1233.

Theander, M., Inganäs, O., Mammo, W., Olinga, T., Svensson, M. & Andersson M. R. (1999), *J. Phys. Chem. B*, **103**, 7771-7780.

Vaschetto, M. E., Retamal, B. A., Monkman, A. P. & Springborg M. (1999), *J. Phys. Chem. A*, **103**, 11096-11103.

Vanhee, S., Rulkens, R., Lehmann, U., Rosenauer, C., Schulze, M., Köhler, W. & Wegner G., (1996), *Macromolecules*, **29**, 5136-5142.

Winokur, M. J. (1998). *Handbook of Conducting Polymers*, edited by T. A. Skotheim., R. L. Elsenbaumer & J. R. Reynolds, pp. 707-726. New York: Marcel Dekker.

Yu, S. M., Conticello, V. P., Zhang, G., Kayser, C., Fournier, M. J., Mason, T. L. & Tirrell, D. A. (1997), *Nature*, **389**, 167-170.